Optics Letters

Mid-infrared photodetectors operating over an extended wavelength range up to 90 K

Yan-Feng Lao,[1] A. G. Unil Perera,[1,2,*] L. H. Li,[3] S. P. Khanna,[3,5] E. H. Linfield,[3] Y. H. Zhang,[4] and T. M. Wang[4]

[1]Department of Physics and Astronomy, Georgia State University, Atlanta, Georgia 30303, USA
[2]Center for Nano-Optics (CeNO), Georgia State University, Atlanta, Georgia 30303, USA
[3]School of Electronic and Electrical Engineering, University of Leeds, Leeds LS2 9JT, UK
[4]Key Laboratory of Artificial Structures and Quantum Control, Department of Physics and Astronomy, Shanghai Jiao Tong University, Shanghai 200240, China
[5]Currently at Physics of Energy Harvesting, CSIR-National Physical Laboratory, New Delhi 110012, India
*Corresponding author: uperera@gsu.edu

Received 5 October 2015; revised 23 November 2015; accepted 23 November 2015; posted 24 November 2015 (Doc. ID 251304); published 8 January 2016

We report a wavelength threshold extension, from the designed value of 3.1 to 8.9 μm, in a *p*-type heterostructure photodetector. This is associated with the use of a graded barrier and barrier offset, and arises from hole–hole interactions in the detector absorber. Experiments show that using long-pass filters to tune the energies of incident photons gives rise to changes in the intensity of the response. This demonstrates an alternative approach to achieving tuning of the photodetector response without the need to adjust the characteristic energy that is determined by the band structure.

OCIS codes: (040.5160) Photodetectors; (040.3060) Infrared; (300.6470) Spectroscopy, semiconductors; (300.6340) Spectroscopy, infrared.

http://dx.doi.org/10.1364/OL.41.000285

In general, the response threshold of a photodetector is determined by a characteristic energy, Δ, which is the minimum energy for a photoexcited carrier to overcome and contribute to the photocurrent. Δ is determined by the highest possible energy state carriers can occupy in the detector absorber, and the potential barrier over which carriers have to pass. The detector threshold can typically be designed by choosing an appropriate potential barrier [1], or by changing the energy distribution of carriers (e.g., adjusting the Fermi level through varying the carrier concentration) [2]. Equally, the dark current is principally determined by thermionic emission, and thus also governed by the value of Δ. This indicates that a higher dark current would be observed in a long-wavelength detector that requires a reduced value of Δ. Therefore, a detector that enables long wavelength detection without changing Δ will offer significant advantages. The concept of wavelength extension was recently demonstrated [3] based on hole–hole interactions and associated energy transfers. The consequence of the interaction was a change in the energy distribution of holes. This was demonstrated experimentally by injecting photoexcited hot holes into the absorber of the detector. A response extending into the very long-wavelength infrared range up to 55 μm was observed; however, the operating temperature was restricted to below 35 K.

In this Letter, we report on the observation of an extended response up to 8.9 μm at 90 K. This *p*-type GaAs/AlGaAs heterojunction detector has a graded barrier and an offset (δE_v) compared to the standard structure [4] [see the VB diagram shown in Fig. 1(a)], designed for 3.1 μm operation. Although this extension is less than that of the previous report (55 μm at 5.3 K) [3], its operation at 90 K demonstrates the potential for high temperature detector development.

By varying the Al fractions, the detector under study has a graded potential profile with an offset between the barriers below and above the absorber. The active region consists of (from top to bottom) a 400 nm-thick undoped $Al_{0.57}Ga_{0.43}As$ constant barrier, an 80 nm-thick *p*-type GaAs absorber (1×10^{19} cm^{-3}), and an 80 nm-thick undoped $Al_xGa_{1-x}As$ graded barrier with x varying linearly from 0.75 (top) to 0.45 (bottom). This active region is sandwiched between two *p*-type GaAs (1×10^{19} cm^{-3}) contact layers. In order to demonstrate the wavelength extension in this sample, another detector sample, LH1002, was also measured [Fig. 1(b)], with a 20 nm-thick and *p*-type doped (1×10^{19} cm^{-3}) GaAs absorber, sandwiched between two symmetrical and flat (60 nm) $Al_{0.57}Ga_{0.43}As$ barriers. The detectors were fabricated by wet etching square mesas, and evaporation of Ti/Pt/Au ohmic contacts onto the top and bottom *p*-type GaAs contact layers (top and bottom contact, referred to as TC and BC, respectively). A top ring contact with a window opened in the center was fabricated to allow front-side illumination. The experiments were carried out on 400 μm × 400 μm mesas with an open area of 260 μm × 260 μm. The spectral response was measured using a Perkin–Elmer system 2000 Fourier Transform InfraRed (FTIR) spectrometer.

A bolometer with known sensitivity was used for background measurements and calibrating the responsivity.

The Fermi level in the p-type GaAs emitter lies at 0.034 eV below the VB top at 80 K, and varies only slightly over the temperature range measured in this study. Therefore, the Fermi level has little effect on the value of Δ and the detection threshold. The threshold is mainly determined by the Al fractions of the graded barrier and the flat barrier (i.e., x_2 and x_3, with corresponding Δ of 0.40 eV and 0.32 eV, respectively) [Fig. 1(a)], for operation under forward and reverse biases, respectively; here, forward bias corresponds to positive bias polarity on the TC.

When holes absorb photons in the absorber, they gain extra momentum and can transport to both directions towards the BC and TC, giving rising to forward and reverse photocurrents, respectively. The process of photoexcited holes escaping over the absorber-barrier interface is known as photoemission [5]. As a consequence, the net photocurrents are determined by the balance of the photoemission efficiencies associated with the holes' forward and reverse movements. There are two factors that come into play for photoemission: the photoexcited hole energy (ε) and the potential barrier Δ, which is determined by the barrier height and applied bias. The photoemission efficiency is proportional to $(\epsilon - \Delta)$ [5].

At 0 V, the forward photocurrent is obtained by photoexcited holes overcoming a potential barrier of 0.40 eV (corresponding to the highest barrier height in the graded barrier region). For the reverse photocurrent, a photoexcited hole needs to escape out of the absorber (towards the TC) and this has to be refilled by another hole coming from the BC. The refilling process requires the hole to overcome the barrier height of 0.40 eV as well. It seems clear that, for operation at 0 V, it is only when the energy of a photon is greater than 0.40 eV, that a response would be expected. However, this expectation was not observed in terms of experimental results, as shown in Fig. 2, where an extra response beyond 3.1 μm (corresponding to 0.40 eV in energy) is observed as a wavelength extension. Although this wavelength extension is obtained up to 90 K, we concentrate here on results at 60 K, as this allows us to study the response behavior better. In terms of the aforementioned carrier transport, there will exist photocurrent cancellation due to both forward and reverse photocurrents passing through the device. The forward photocurrent is dominant for the spectral range between 1 and 3 μm, while reverse photocurrent is dominant for the spectral range between 3 and 12 μm. The photoemission efficiency and hence this cancellation depends on the bias, which is seen as a zero spectral response point shifting between 2.9 and 4.2 μm when the bias is between −0.4 ∼ 0.7 V.

To understand the spectral response, temperature-dependent internal photoemission spectroscopy (TDIPS) [5] was used to obtain the behavior of the photoemission threshold at different biases. The quantum yield, defined as the number of collected photoexcited holes per incident photon, is proportional to the multiplication of the spectral responsivity with photon energy [5]. The details of the TDIPS principle and the formalism for interpreting yield spectra by a fitting procedure are described in Refs. [5,6]. Figure 3 (a) plots the TDIPS fitting results in the near-threshold regime. From the fittings, threshold energies at different biases are obtained, as shown in Fig. 3(b) (■, ▼), along with a comparison to the value of Δ obtained from Arrhenius plots (□), derived from measurements of current-bias-temperature (I-V-T) characteristic under dark conditions. It is notable that for voltages between −0.6 ∼ −3.8 V, good agreement with the experiment can be achieved by modeling the system using two photoemission processes [as illustrated in the inset of Fig. 3(a)], each of which can be fitted with an individual threshold energy. The thresholds with low-energy values agree with those obtained by single-threshold TDIPS fittings. As discussed below, they originate from the wavelength extended response. In contrast, the high-energy thresholds are associated from "normal" response, where the threshold is determined by Δ.

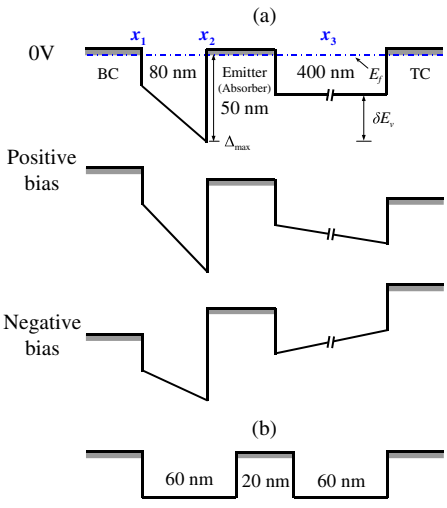

Fig. 1. (a) The unbiased VB diagram of a graded barrier structure (sample SP1007), where the emitter (absorber), top and bottom contacts are p-type GaAs. x_1 (0.45), x_2 (0.75), and x_3 (0.57) are mole fractions of aluminum in the AlGaAs barriers, and δE_v (0.1 eV) is the offset between the barriers below and above the emitter. Δ_{max} is determined to be 0.4 eV by Arrhenius plots at 0 V, in agreement with the designed value. The VB diagrams under positive and negative biases are also shown. (b) The VB diagram of sample LH1002, which consists of two AlGaAs barriers with the same thickness (60 nm) (i.e., $x_1 = x_2 = x_3 = 0.57$).

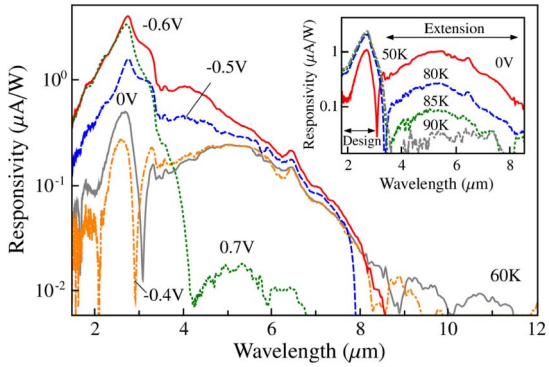

Fig. 2. Spectral response measured at 60 K. The spectral profile varying with bias between −0.4 ∼ 0.7 V is due to the presence of the zero-response point (between 2.9–4.2 μm) where the negative and positive photocurrents cancel. The inset plots the photovoltaic (0 V) response up to a maximum temperature of 90 K.

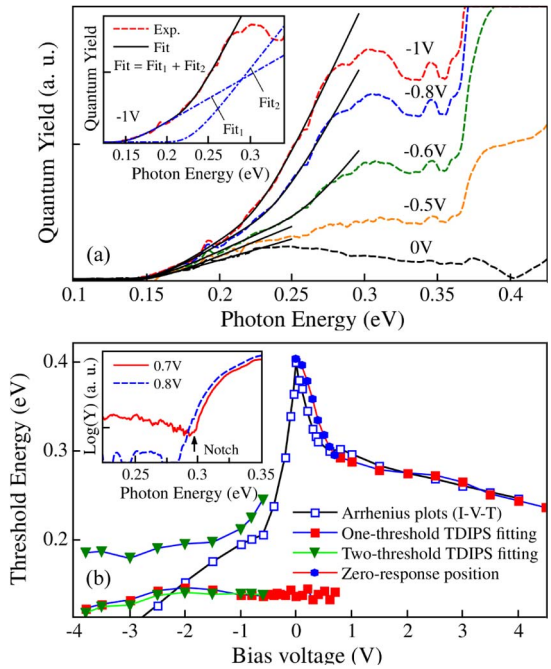

Fig. 3. (a) Quantum yield spectra and fittings by TDIPS [5]. For (negative) biases (greater than 0.6 V), the TDIPS fittings are composed of two components (i.e., Fit_1 and Fit_2) as shown in the inset; each of them was fitted with an individual threshold energy. (b) Comparison of the values of Δ obtained by Arrhenius plots and TDIPS fittings. Δ = 0.40 eV at 0 V is consistent with the structure design (see Fig. 1). Inset: the zero-response point disappears when the bias increases beyond 0.8 V.

The value of Δ at 0 V is 0.40 eV, agreeing with the expected value for a *p*-type $GaAs/Al_{0.75}Ga_{0.25}As$ junction. Such agreement between the spectral response and the structure parameters is typically found to be good [5]. However, the measurement of spectral response as shown in Fig. 2(a) indicates a wavelength extension beyond 3.1 μm and up to 8.9 μm, which has a corresponding threshold energy much less than the values determined from Arrhenius plots at biases down to −2 V [see Fig. 3(b)].

The threshold energies obtained by TDIPS fittings display three distinct features: (1) low (negative and positive) bias operation, where the spectral threshold energies (i.e., 0.14 eV in energy or 8.9 μm in wavelength) are independent of bias; (2) large negative bias (with magnitude >2 V), where the fitted threshold energy is greater than the Arrhenius value [5]; and (3) high positive bias, where at >0.7 V the threshold energy jumps to a high value beyond which the threshold energies extracted from the response spectra agree with those obtained from Arrhenius plots. We thus ascribe the wavelength extension in spectral response as occurring between $-2.0 \sim 0.7$ V.

The wavelength extension under positive bias originates from a negative photocurrent coexisting with the positive photocurrent, as can be seen from the occurrence of the zero-response point shown in the inset of Fig. 3(b). At voltages >0.8 V, the negative photocurrent is negligible, leaving only the positive photocurrent being measured. This is further supported by the agreement of the zero-response point with the activation energies from Arrhenius plots, as shown in Fig. 3(b). The zero-response position can thus be considered as the onset of the positive response, and thus should be, in accordance with the threshold energy, measured under positive biases and in dark conditions.

It is beneficial to increase the operating temperature of a device, for example, up to room temperature. Reference [3] reported a very long-wavelength extension, but with a limit of operating temperatures up to 35 K. Although the very long-wavelength response is greatly reduced and eventually becomes unresolvable at >35 K, photoresponse in the mid-infrared range is still observed up to 90 K, as shown in the inset of Fig. 2, which plots the response at 0 V. This also indicates that this detector is capable of operating in the photovoltaic mode [7–9], owing to the asymmetric structure configuration, which

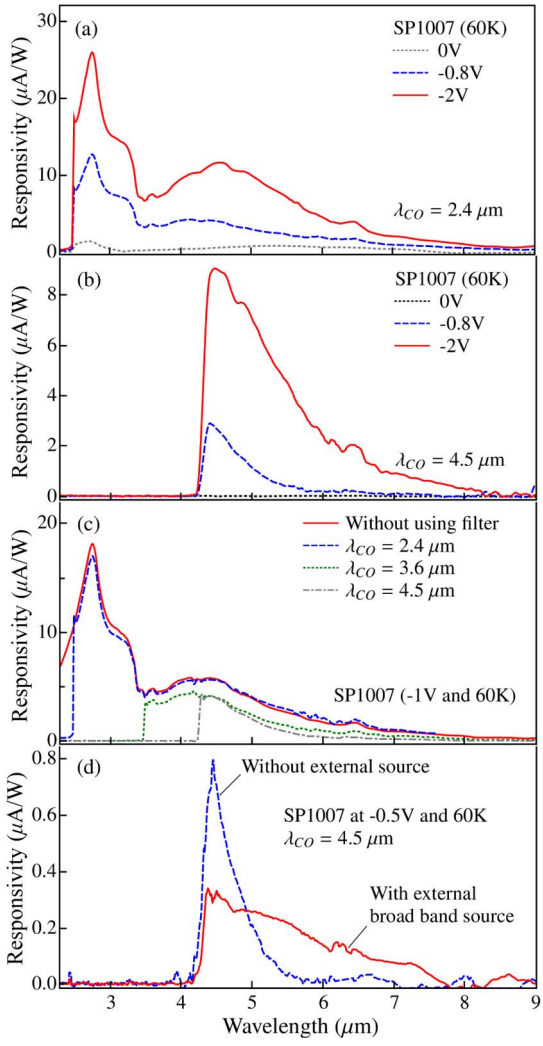

Fig. 4. Response spectra (60 K) measured by using long-pass filters with cut-on wavelengths (λ_{CO}) of (a) 2.4 μm, and (b) 4.5 μm. A response at 0 V is observed with the 2.4 μm filter, while it is disabled by using a 4.5 μm filter. (c) Spectral response for different λ_{CO} values. The extended wavelength responsivity reduces as λ_{CO} increases. The TDIPS fitting confirms that the response threshold remains the same. (d) Comparison of the response measured using a 4.5 μm long-pass filter, with and without an external red lamp as the optical excitation source.

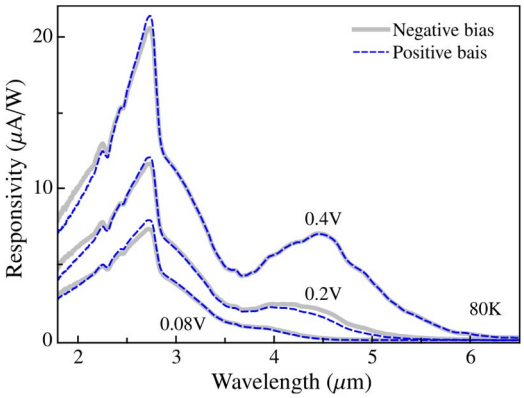

Fig. 5. Spectral response of sample LH1002, which has a symmetric band configuration with flat barriers beside the emitter (i.e., $\delta E_v = 0$). A study of the band offset on this sample is reported in Ref. [10].

leads to hole accumulation at the top contact at 0 V under illumination.

The response threshold is determined by the energies of the holes in the emitter and the VB offset of the GaAs/AlGaAs junction. As the VB offset only changes slightly with temperature [5], a change in the hole distribution is the main cause of the observed response extension. Figures 4(a)–4(d) demonstrate tuning of the response by using long-pass filters and an external optical excitation source.

The use of long-pass filters varies the energies of incident photons and hence the energies of the carriers [3]. One approach is to disable high-energy photons from the FTIR spectrometer from being incident onto the sample, thus disabling wavelength extension. For example, a filter with cut-on wavelength of 4.5 μm [Fig. 4(b)] disables the 3.1–8.9 μm photovoltaic response (at zero-bias operation). The increase of the response threshold wavelength at higher bias is then due to image-force barrier lowering [5]. Figure 4(c) shows that the responsivity in the long-wavelength region decreases as the cut-on wavelength of the long-pass filter is increased. However, the wavelength threshold as confirmed by the TDIPS fittings remains the same. Figure 4(d) demonstrates that an external optical excitation source can be used to enable a wavelength-extended response to be recovered, because the external optical excitation source provides high-energy hole injection into the emitter. All of these observations are consistent with an explanation based on hole interactions, which lead to a change in hole energy distribution, causing the wavelength extension.

The observed wavelength extension is a consequence of carrier transport in a device with asymmetrical band configuration (i.e., an offset in the barriers below and above the absorber). This conclusion is confirmed by measuring a reference sample, LH1002, which has a symmetrical band alignment with flat barriers neighboring the emitter. As shown in Fig. 5, the response of LH1002 is nearly the same for negative and positive biases. A prior investigation [10] of the band offset shows that the response threshold energies are consistent with the designed structural parameters. No response threshold extension is observed for sample LH1002.

The photoexcited holes are required to undergo a photoemission process at the emitter-barrier interface in order to contribute to photocurrents. The photoemission process means a transfer from the VB of the emitter to that of the barrier, which can be accomplished via hole-phonon scattering events. The temperature dependence of the extended response (inset of Fig. 2) implies significant damping of the scattering at 90 K and beyond. In addition, observing a photoresponse with wavelength extension means that carriers are responding to low-energy photons; this takes place when carriers (holes in this case) are first excited (for example, through carrier–carrier scattering [3]) into high-energy states before the photoresponse occurs. Although such a photoresponse mechanism is consistent with our observations (including extension enabled by an external broad band source), direct evidence of such hot-carrier dynamics has still to be obtained.

To conclude, the response threshold for a GaAs/$Al_xGa_{1-x}As$ photodetector with a designed threshold wavelength of 3.1 μm (at 0 V) has been measured. We observed an extended response up to the mid/long-wave infrared range. The tunability of the wavelength extended response is demonstrated by using an external optical excitation source. It is found that the detector operates up to a temperature of 90 K, which opens up the prospect of designing photodetectors operating up to high temperatures.

Funding. Army Research Office (ARO) (W911NF-15-1-0018); Engineering and Physical Sciences Research Council (EPSRC) (UK); European Research Council (ERC) (TOSCA); National Natural Science Foundation of China (NSFC) (91221201); National Science Foundation (NSF) (ECCS-1232184).

REFERENCES

1. H. Schneider and H. C. Liu, *Quantum Well Infrared Photodetectors: Physics and Applications*, Vol. **126** of Springer Series in Optical Sciences (Springer, 2007).
2. A. G. U. Perera, *Advances in Infrared Photodetectors*, Vol. **84** of Semiconductors and Semimetal Series (Elsevier, 2011).
3. Y.-F. Lao, A. G. U. Perera, L. H. Li, S. P. Khanna, E. H. Linfield, and H. C. Liu, Nat. Photonics **8**, 412 (2014).
4. P. V. V. Jayaweera, S. G. Matsik, A. G. U. Perera, H. C. Liu, M. Buchanan, and Z. R. Wasilewski, Appl. Phys. Lett. **93**, 021105 (2008).
5. Y.-F. Lao and A. G. U. Perera, Phys. Rev. B **86**, 195315 (2012).
6. Y.-F. Lao, P. K. D. D. P. Pitigala, A. G. Unil Perera, E. Plis, S. S. Krishna, and P. S. Wijewarnasuriya, Appl. Phys. Lett. **103**, 181110 (2013).
7. A. Rogalski, Infrared Phys. Technol. **41**, 213 (2000).
8. H. Schneider, C. Schönbein, M. Walther, K. Schwarz, J. Fleissner, and P. Koidl, Appl. Phys. Lett. **71**, 246 (1997).
9. A. V. Barve and S. Krishna, Appl. Phys. Lett. **100**, 021105 (2012).
10. Y.-F. Lao, A. G. Unil Perera, Y. H. Zhang, and T. M. Wang, Appl. Phys. Lett. **105**, 171603 (2014).